EUROPEAN ORGANIZATION FOR NUCLEAR RESEARCH

CERN-PPE/97-XX
July 15, 1997

Missing mass spectra in hadronic events from e^+e^- collisions at $\sqrt{s} = 161 \div 172$ GeV and limits on invisible Higgs decays

The L3 Collaboration

Abstract

Events characterised by large hadronic energy and transverse momentum are selected from the data collected by the L3 detector at LEP at centre-of-mass energies between 161 and 172 GeV, corresponding to an integrated luminosity of 21 pb^{-1}. The visible mass and the missing mass distributions of the selected events are consistent with those expected from Standard Model processes. This result is combined with that from data taken at the Z resonance to set an upper limit on the production rate and decay into invisible final states of a non-minimal Higgs boson, as a function of the Higgs mass. Assuming the non-minimal Higgs production cross section to be the same as for the Standard Model Higgs boson and the decay branching fraction into invisible final states to be 100%, a Higgs mass lower limit of 69.6 GeV is derived at 95% confidence level.

Submitted to *Phys. Lett. B*

1 Introduction

This paper reports on the results of a study of hadronic events, with large visible energy, visible mass and transverse momentum, from the data collected by the L3 experiment at $\sqrt{s} = 161 \div 172$ GeV. The idea here is to identify events with a Z decaying hadronically recoiling against missing energy and momentum due to undetected particles. If a particle is produced in association with the Z and decays into invisible particles, then a peak in the missing mass spectrum should be observed. The kinematic region investigated here is different from those investigated in other studies of hadronic events with missing energy and momentum, such as the one for the measurement of the Weν cross section [1] as well as the the search for the Standard Model Higgs boson, H_{SM}, in the $ZH_{SM} \to \nu\bar{\nu}q\bar{q}$ channel [2] and supersymmetric particle searches [3].

Non-Standard Model processes could produce an unexpected excess of events in the spectrum of the missing mass recoiling to the Z. One example is the production of a non-minimal Higgs boson, h, decaying into invisible particles, in association with a hadronically decaying Z boson. Examples of invisible particles which a non-minimal Higgs could decay to are light neutralinos [4] in the context of supersymmetric extensions of the Standard Model; or Majorons [5], in so called Majoron models, used to generate neutrino masses.

2 Data and Monte Carlo samples

We use data corresponding to integrated luminosities of 10.8, 1.0 and 9.2 pb^{-1} collected by the L3 detector [6] at LEP at centre-of-mass energies, $\sqrt{s}$, of 161.3, 170.3 and 172.3 GeV, respectively. For the signal efficiency studies a sample of Higgs events has been generated using PYTHIA [7], imposing 100% decay branching fraction of the Higgs boson into invisible particles. About 3500 Higgs events, with hadronic Z decay, were simulated for each Higgs mass value investigated. The Standard Model cross section for Higgs production is calculated using the HZHA generator [8]. For the study of fermion pair and four-fermion productions the following Monte Carlo generators were used: PYTHIA ($e^+e^- \to q\bar{q}(\gamma)$), KORALW [9] ($e^+e^- \to W^+W^-$), PYTHIA and PHOJET [10] ($e^+e^- \to e^+e^-q\bar{q}$), and EXCALIBUR [11] ($e^+e^- \to f\bar{f}'f\bar{f}'$). The number of simulated fermion pair and four-fermion events corresponds to at least 100 times the collected luminosity.

The L3 detector response is simulated using the GEANT 3.15 [12] program, which takes into account the effect of energy loss, multiple scattering and showering in the detector. The GHEISHA [13] program is used to simulate hadronic interactions in the detector.

3 Event properties

Higgs events, produced via the Higgs-strahlung process $e^+e^- \to Zh$, with $Z \to q\bar{q}$ and $h \to$ invisible particles, and Standard Model Higgs events, produced via the same process, $e^+e^- \to ZH_{SM}$, with $Z \to \nu\bar{\nu}$ and $H_{SM} \to q\bar{q}$, have similar signature: large visible energy, two acoplanar hadronic jets, large tranverse momentum and absence of isolated leptons.

However, at present centre-of-mass energies, the Z boson is produced almost at rest, thus for invisibly decaying Higgs events the visible energy and visible mass are close to the Z mass, independently of the Higgs mass. This is not the case for Standard Model Higgs events, where the visible energy and visible masses are generally below the Z mass (in the Higgs mass range investigated at present energies), and depend upon the Higgs mass. Furthermore, b-tagging is not as efficient in selecting invisibly decaying Higgs events as in the Standard Model Higgs search, since only about 15% of the total number of Higgs events will contain a $\mathrm{b\bar{b}}$ pair (from the Z) as compared to about 87% of the total Standard Model Higgs events. Thus the analysis is based only on kinematic cuts and does not make use of b-tagging.

Hadronic events with large visible energy and momentum also originate from Standard Model processes, such as quark pair production ($\mathrm{e^+e^-} \to \mathrm{q\bar{q}}(\gamma)$) and four-fermion production, involving charged gauge boson exchange ($\mathrm{W^+W^-}$ and $\mathrm{We}\nu$ production) and neutral gauge boson exchange ($\mathrm{Z}/\gamma^*\mathrm{Z}/\gamma^*$ and Zee production). The missing energy and momentum in these events is either genuine (e.g. in $\mathrm{W^+W^-}$ events, when one W decays into lepton+neutrino) or results from energy mis-measurement and incomplete detector coverage. The most important sources of background in this search are $\mathrm{q\bar{q}}(\gamma)$, $\mathrm{W^+W^-}$ and $\mathrm{We}\nu$ events. The first two have a relatively large production cross section (129 pb and 12.3 pb respectively for $\mathrm{q\bar{q}}(\gamma)$ and $\mathrm{W^+W^-}$ cross sections at 172 GeV), while the third, despite its relatively small production cross section (0.35 and 0.45 pb at 161 and 172 GeV respectively), gives a relatively large contribution in the same kinematic region as the Higgs signal.

4 Event selection

First we select hadronic events with large visible energy, small longitudinal imbalance, and small energy in the forward calorimeters to suppress the two-photon contribution $\mathrm{e^+e^-} \to \mathrm{e^+e^-q\bar{q}}$ and reduce the $\mathrm{q\bar{q}}(\gamma)$ contribution, when the photon is in the forward region of the detector or escapes in the beam pipe. Then we apply additional requirements to further reduce the $\mathrm{q\bar{q}}(\gamma)$ and $\mathrm{W^+W^-}$ contributions and select events with visible energy, momentum and mass consistent with a Z decaying into hadrons and recoiling against undetected particle. As we reduce the event sample we compare the observed spectra of the visible mass, calculated from the visible energy E_{vis} and momentum P_{vis}, $M_{\mathrm{vis}} = (E_{\mathrm{vis}}^2 - P_{\mathrm{vis}}^2)^{1/2}$ and the missing mass $M_{\mathrm{mis}} = (s + M_{\mathrm{vis}}^2 - 2\sqrt{s}E_{\mathrm{vis}})^{1/2}$, to the contributions from Standard Model fermion pair and four-fermion productions.

The quantities used in the selection are as follows: number of tracks, N_{T}; number of calorimetric clusters, N_{C}; the visible energy, $E_{\mathrm{vis}}/\sqrt{s}$; longitudinal and transverse imbalances, $|P_{\|}|/E_{\mathrm{vis}}$ and $P_{\perp}/E_{\mathrm{vis}}$, respectively; the total energy deposition in the electromagnetic calorimeter, E_{em}; energy deposition in the luminosity monitor, E_{v4}; energy deposition in the forward lead-scintillator calorimeter, E_{v8}; the relative energy in a cone of 30° around the beam direction, $E_{\mathrm{v30}}/E_{\mathrm{vis}}$; the larger of the two jet masses, $\max(M_{\mathrm{j1}}, M_{\mathrm{j2}})$, when the event is forced into two jets using DURHAM algorithm [14]; the sum of the angles between

the jets, θ_{123}, when the event is forced into three jets using the DURHAM algorithm; the energy deposition in $\pm 25^\circ$ of the missing momentum direction in the plane transverse to the beam, $E_{25}^{\perp}$; the number of high energy isolated leptons, $N_{i\ell}$, i.e. leptons (e, μ, τ) with energy $E_\ell > 5$ GeV and isolation $I_\ell < 1$ GeV, where I_ℓ is the energy deposition in the region between 10° and 30° half opening angle around the lepton direction.

The following cuts are applied in order to reduce the Standard Model contributions, mainly from $q\bar{q}(\gamma)$ and W^+W^- productions:

1) Hadronic preselection: $N_C > 14$, $N_T > 4$, $E_{em} > 10$ GeV, $E_{v4} < 5$ GeV, $E_{v8} < 10$ GeV, $0.4 < E_{vis}/\sqrt{s} < 1$, $|P_\parallel|/E_{vis} < 0.5$;

2) $E_{v30}/E_{vis} < 0.5$;

3) $E_{vis}/\sqrt{s} < 0.7$;

4) $|P_\parallel|/E_{vis} < 0.3$;

5) $\max(M_{j1}, M_{j2}) < 40$ GeV;

6) $\theta_{123} < 349^\circ$ for $\sqrt{s} = 172$ GeV or $\theta_{123} < 355^\circ$ for $\sqrt{s} = 161$ GeV;

7) $P_\perp/E_{vis} > 0.1$;

8) $N_{i\ell} = 0$ and $E_{25}^{\perp} < 12$ GeV.

The distributions of the transverse imbalance, the maximum jet mass, the visible mass and the missing mass are shown in Figures 1(a) through 1(d) after the hadronic preselection (cut 1), for the data, the Standard Model expectation and, for comparison, a 70 GeV Higgs signal at $\sqrt{s} = 172$ GeV. At this centre-of-mass energy, after the hadronic preselection, 554 events are observed in the data, while 564 events are expected from Standard Model processes: 83% from $q\bar{q}\gamma$ production, 16% from W^+W^- production and the remaining 1% from Weν, Zee and $Z/\gamma^*Z/\gamma^*$ production. At $\sqrt{s} = 161$ GeV 791 events are observed with 778 expected from Standard Model processes: 96% from $q\bar{q}\gamma$, 3% from W^+W^-, and 1% from Weν, Zee, and $Z/\gamma^*Z/\gamma^*$ production. The Higgs signal efficiency is 95%: 5.1 Higgs events are expected at 172 GeV and 1.2 at 161 GeV, for 70 GeV Higgs mass, assuming Standard Model cross section for Higgs production via $e^+e^- \to Zh$ process.

The selection progressively reduces the $q\bar{q}(\gamma)$ contribution and to a lesser extent the W^+W^- and Weν contributions. The most effective requirements to reduce the latter are the jet mass cut (cut 5), the θ_{123} angle cut (cut 6), the absence of isolated high energy leptons and the isolation of the missing energy (cut 8). The jet mass cut and the θ_{123} angle cut, in particular, are very effective at reducing the W^+W^- contribution when one W decays hadronically and the other into a neutrino plus a tau. If the tau is not identified, it is included in one of the two jets when the event is reconstructed into two jets. Thus one of the two jet masses is high compared to genuine two-jet events. Similarly, when the $qq\tau\nu$ event is reconstructed into three jets it is likely to have a value of θ_{123} larger than for a genuine two-jet event.

The number of events observed, after sequentially applying the selection cuts, compared to the expected Standard Model contributions, is shown in Fig. 2. Good agreement between the data and the Standard Model expectation is found in the subsequent steps of the selection. For comparison, the number of events expected for two invisible Higgs masses, assuming Standard Model Higgs production cross section, is also given in Fig. 2.

In Fig. 3 the distributions of $M_{\rm vis}$ and $M_{\rm mis}$, after selection cuts 1 through 6, are shown at centre-of-mass energies of 161 and 172 GeV. At this stage of the analysis, at $\sqrt{s} = 172$ GeV 21 events are observed in the data, while 20.7 events are expected from Standard Model processes: 47% from $\rm q\bar{q}\gamma$ events, 48% from $\rm W^+W^-$ events and 5% from Zee, $\rm Z/\gamma^*Z/\gamma^*$ and Weν events. At $\sqrt{s} = 161$ GeV 35 events are observed with 25.1 expected from Standard Model processes: 81% from $\rm q\bar{q}\gamma$, 13% from $\rm W^+W^-$, and 6% from Zee, $\rm Z/\gamma^*Z/\gamma^*$ and Weν production. At this stage of the selection, the Higgs signal efficiency is 63% for a 65 GeV Higgs at $\sqrt{s}$=161 GeV and 62% for a 70 GeV Higgs at $\sqrt{s}$=172 GeV.

For the Higgs events, the visible mass is centered about the Z mass, with a Z mass resolution $\sigma_{\rm Z}$ of about 9 GeV, and the missing mass is centered about the Higgs mass, with a resolution which ranges from 15 to 12 GeV for Higgs masses between 60 and 70 GeV at $\sqrt{s} = 172$ GeV. A better resolution in the Higgs mass is obtained by imposing the constraint that the visible energy and momentum comes from the Z decay, and determining the Higgs energy from rescaling the measured missing energy, imposing total energy and momentum constraints. The expression for the reconstructed Higgs mass, $\rm M_{rh}$, is

$$M_{\rm rh} = \frac{\sqrt{s} - [s - (s - (M'_{\rm Z})^2)(1 - \beta^2_{\rm mis})]^{1/2}}{[1 - \beta^2_{\rm mis}]^{1/2}} \ .$$

Here $\beta_{\rm mis} = P_{\rm vis}/(\sqrt{s} - E_{\rm vis})$ is, in the Higgs events, the measured Higgs velocity. The quantity $M'_{\rm Z} = M_{\rm Z} + (M_{\rm vis} - M_{\rm Z})\Gamma_{\rm Z}/\sigma_{\rm Z}$ is used rather than the Z mass, $M_{\rm Z}$, to take into account the finite Z width, $\Gamma_{\rm Z}$. The resolution of $M_{\rm rh}$ ranges from 5.9 GeV for a 60 GeV Higgs to 3.6 GeV for a 70 GeV Higgs [15] at $\sqrt{s}$=172 GeV.

5 Results and conclusions

The distributions of $M_{\rm vis}$, $M_{\rm mis}$ and $M_{\rm rh}$, after applying final selection (cuts 1 through 8), are shown in Fig. 4 for the data and the Standard Model contributions. Also shown (dashed histogram) is the expected contribution from a 70 (65) GeV Higgs at $\sqrt{s} = 172$ (161) GeV, normalised to the actual luminosity using the Standard Model Higgs production cross section, added to the contributions from Standard Model processes. The values of $M_{\rm vis}$, $M_{\rm mis}$ and $M_{\rm rh}$ for the data events surviving the final selection are given in Table 1. No significant excess over the expected Standard Model contributions is observed in the measured mass distributions.

The observed number of events and the expected contributions from Standard Model processes are compared in Table 2 after final selection. In total we expect 3.4±0.4 and 6.0±0.6 events from Standard Model physics processes and we observe 3 and 5 events at $\sqrt{s}$= 161 and 172 GeV, respectively.

Observed event	$M_{\rm vis}$(GeV)	$M_{\rm mis}$(GeV)	$M_{\rm rh}$(GeV)
$\sqrt{s}$=172 GeV			
# 1	72 ± 9	62 ± 9	50 ± 4
# 2	80 ± 8	57 ± 9	50 ± 4
# 3	71 ± 9	79 ± 8	61 ± 4
# 4	82 ± 8	82 ± 8	72 ± 3
# 5	82 ± 8	80 ± 8	70 ± 3
$\sqrt{s}$=161 GeV			
# 1	89 ± 9	< 4	< 4
# 2	73 ± 9	79 ± 8	60 ± 4
# 3	81 ± 8	75 ± 8	64 ± 4

Table 1: The values of the visible mass, the missing mass and the reconstructed Higgs mass for the data events passing the final selection.

SM processes	$\sqrt{s}$=161 GeV	$\sqrt{s}$=172 GeV
$q\bar{q}$	1.15 ± 0.13	0.32 ± 0.06
Zee	0.003 ± 0.002	0.003 ± 0.002
$Z/\gamma^*Z/\gamma^*$	0.028 ± 0.007	0.053 ± 0.005
Weν	0.90 ± 0.05	0.68 ± 0.07
W^+W^-	1.34 ± 0.06	5.02 ± 0.11
Total expected	$3.40 \pm 0.15(stat)$	$6.00 \pm 0.15(stat)$
Total observed	3	5

Table 2: The number of events observed after final selection in the data collected at centre-of-mass energies between 161 and 172 GeV, compared to the number of expected events from Standard Model processes. The quoted errors on the Monte Carlo expectations are statistical only. The systematic errors are discussed in the text.

The error on the Standard Model expectation includes the error from limited Monte Carlo statistics, which amounts to 4% (see Table 2), and the error on the selection efficiency. The latter is mainly due to energy calibration uncertainties and it has been estimated by repeating the analysis with the global energy scale changed by $\pm$ 3% and the energy scales of the individual subdetectors by $\pm$5 % [2]. Thus, a total error of about 10% is estimated to affect the Standard Model expectation.

The efficiencies for an invisibly decaying Higgs signal as a function of the Higgs mass are reported in Table 3 together with the number of $e^+e^- \to Zh$ expected events, assuming Standard Model Higgs production cross section, $\sigma(ZH_{\rm SM})$, and 100% branching fraction of the Higgs boson into invisible final states. A total error of about 4% affects the signal efficiencies, including both the uncertainty from limited Monte Carlo statistics ($\lesssim$ 2%) and the one due to energy calibration uncertainty (2.5 to 3.5% depending on the Higgs mass).

	$\sqrt{s} \approx 91$ GeV		$\sqrt{s}$=161 GeV		$\sqrt{s}$=172 GeV	
Higgs mass (GeV)	$\epsilon_{\mathrm{Zh}}(\%)$	N	$\epsilon_{\mathrm{Zh}}(\%)$	N	$\epsilon_{\mathrm{Zh}}(\%)$	N
50	39	47.5	47	5.87	43	4.53
60	38	11.4	48	3.77	46	3.70
65	36	4.55	42	2.10	47	3.15
67	35	2.99	37	1.36	48	2.94
69	33	1.87	29	0.581	45	2.48
70	32	1.46	28	0.362	46	2.40
71	31	1.12	27	0.230	45	2.11
73	30	0.64	24	0.100	45	1.87

Table 3: Efficiencies, ϵ_{Zh}, and corresponding number of expected events, N, after selection, for the Zh signal, assuming the Zh production cross section to be the same as for the Standard Model Higgs and decay branching fraction into invisible particles to be 100%. The efficiencies for $\sqrt{s} = 161 \div 172$ GeV are affected by a 4% total uncertainty and for LEP1 they are affected by a 3% total uncertainy. No invisibly decaying Higgs candidates were selected from the data collected at the Z resonance [17].

A confidence level calculation, which includes the errors on signal and background expectations, is done according to the method proposed in Ref. [16]. The M_{rh} distributions (see Fig. 4(c) and (f)) for the data, the Standard Model background and the Higgs signal, for several Higgs mass values, are used in the calculation of the confidence level. Combining the $161 \div 172$ GeV results with those from LEP1 [17], a lower limit (Fig. 5(a)) is set on the mass of an invisibly decaying Higgs boson at 95% confidence level

$$m_{\mathrm{h}} > 69.6 \text{ GeV},$$

assuming that the Higgs production cross section $\sigma(\mathrm{Zh})$ is the same as for the Standard Model Higgs and the Higgs branching fraction into invisible particles, BR(h $\rightarrow$ invisible particles), is 100%.

The $\mathrm{e^+e^-} \rightarrow \mathrm{Zh}$ production cross section and the branching fraction into visible and invisible final states of a non-minimal Higgs boson h are model dependent. Thus we set an experimental upper limit on the rate of invisible Higgs final states, relative to the Standard Model Higgs rate, $R_{\mathrm{inv}} = \sigma(\mathrm{Zh})BR(\mathrm{h} \rightarrow \text{invisible particles})/\sigma(\mathrm{ZH_{SM}})$, as a function of the Higgs mass. This limit, which can be used to bound the parameter space of the different models predicting invisible Higgs decays, is shown in Fig. 5(b) for Higgs masses above 50 Gev, where the $161 \div 172$ GeV results improve the LEP1 limit on R_{inv}. The hatched area in Fig. 5(b) is excluded at 95% confidence level.

In conclusion, these results improve on those obtained in previous analyses at LEP1 [17, 18, 19] and are the first ones reported at $\sqrt{s} = 161 \div 172$ GeV concerning invisible Higgs decays.

Acknowledgements

We wish to express our gratitude to the CERN Accelerator Divisions for the good performance of the LEP machine. We acknowledge the efforts of the engineers and technicians who have participated in the construction and the maintenance of this experiment.

References

[1] L3 Collaboration, M. Acciarri *et al.*, "Production of Single W Bosons at LEP" , CERN-PPE/97-28, submitted to Phys. Lett. B.

[2] L3 Collaboration, M. Acciarri *et al.*, "Search for the Standard Model Higgs Boson in e^+e^- collisions at $161 \leq \sqrt{s} \leq 172$ GeV", submitted to Phys. Lett. B.

[3] L3 Collaboration, M. Acciarri *et al.*, "Searches for Charginos, Neutralinos and Sleptons at $\sqrt{s} = 161 \div 172$ GeV", in preparation.

[4] K. Griest, H.E. Haber, Phys. Rev. **D 37** (1988) 719. A. Djouadi, P. Janot, J. Kalinowski, P.M. Zerwas, Phys. Lett. **B 376** (1996) 220.

[5] A.S. Joshipura, J.W.F. Valle, Nucl. Phys. **B 397** (1993) 105;
F. de Campos, O.J. Eboli, J. Rosiek, J.W.F. Valle, Phys. Rev. **D 55** (1997) 1316.

[6] L3 Collaboration, B. Adeva *et al.*, Nucl.Instr.Meth. **A289** (1990) 35; J.A. Bakken *et al.*, Nucl.Instr.Meth. **A275** (1989) 81; O. Adriani *et al.*, Nucl.Instr.Meth. **A302** (1991) 53; B. Adeva *et al.*, Nucl.Instr.Meth. **A323** (1992) 109; K. Deiters *et al.*, Nucl.Instr.Meth. **A323** (1992) 162; M. Chemarin *et al.*, Nucl.Instr.Meth. **A349** (1994) 345; B. Acciari *et al.*, Nucl.Instr.Meth. **A351** (1994) 300; G. Basti *et al.*, Nucl.Instr.Meth. **A374** (1996) 293; A. Adam *et al.*, Nucl.Instr.Meth. **A383** (1996) 342.

[7] T. Sjöstrand, CERN-TH/7112/93 (1993), revised August 1995; T. Sjöstrand, Comp.Phys.Comm. 82 (1994) 74.

[8] P. Janot, "The HZHA generator", in "Physics at LEP2", Eds. G. Altarelli, T. Sjöstrand and F. Zwirner, CERN 96-01 (1996) Vol.2, 309.

[9] M. Skrzypek *et al.*, Comp. Phys. Comm. **94** (1996) 216; M. Skrzypek *et al.*, Phys. Lett. **B372** (1996) 289.

[10] R. Engel, Z. Phys. **C66** (1995) 203; R. Engel, J. Ranft and S. Roesler, Phys. Rev. **D52** (1995) 1459.

[11] F.A. Berends, R. Kleiss and R. Pittau, Nucl. Phys. **B 424** (1994) 308; Nucl. Phys. **B 426** (1994) 344; Nucl. Phys. (Proc. Suppl.) **B 37** (1994) 163; Phys. Lett. **B 335** (1994) 490; R. Kleiss and R. Pittau, Comp. Phys. Comm. **83** (1994) 14.

[12] R. Brun *et al.*, preprint CERN DD/EE/84-1 (Revised 1987).

[13] H. Fesefeldt, RWTH Aachen Report PITHA 85/02 (1985).

[14] S. Catani *et al.*, Phys. Lett. **B 263** (1991) 491; S. Bethke *et al.*, Nucl.Phys. **B 370** (1992) 310.

[15] M. Felcini, L3 Higgs Working Group, L3 internal note 2073, March 97 [1].

[16] V.F. Obratsov, Nucl. Instr. Meth. **A 316** (1993) 388.

[17] L3 Collaboration, M. Acciarri *et al.*, Phys. Lett. **B 385** (1996) 454.

[18] OPAL Collaboration, G. Alexander *et al.*, Phys. Lett. **B 377** (1996) 273.

[19] ALEPH Collaboration, D. Buskulic *et al.*, Phys. Lett. **B 313** (1993) 549.

[1] This L3 Note is freely available on request from: The L3 secretariat, CERN, CH–1211 Geneva 23, Switzerland. Internet: http://hpl3sn02.cern.ch/l3pubanddoc.html

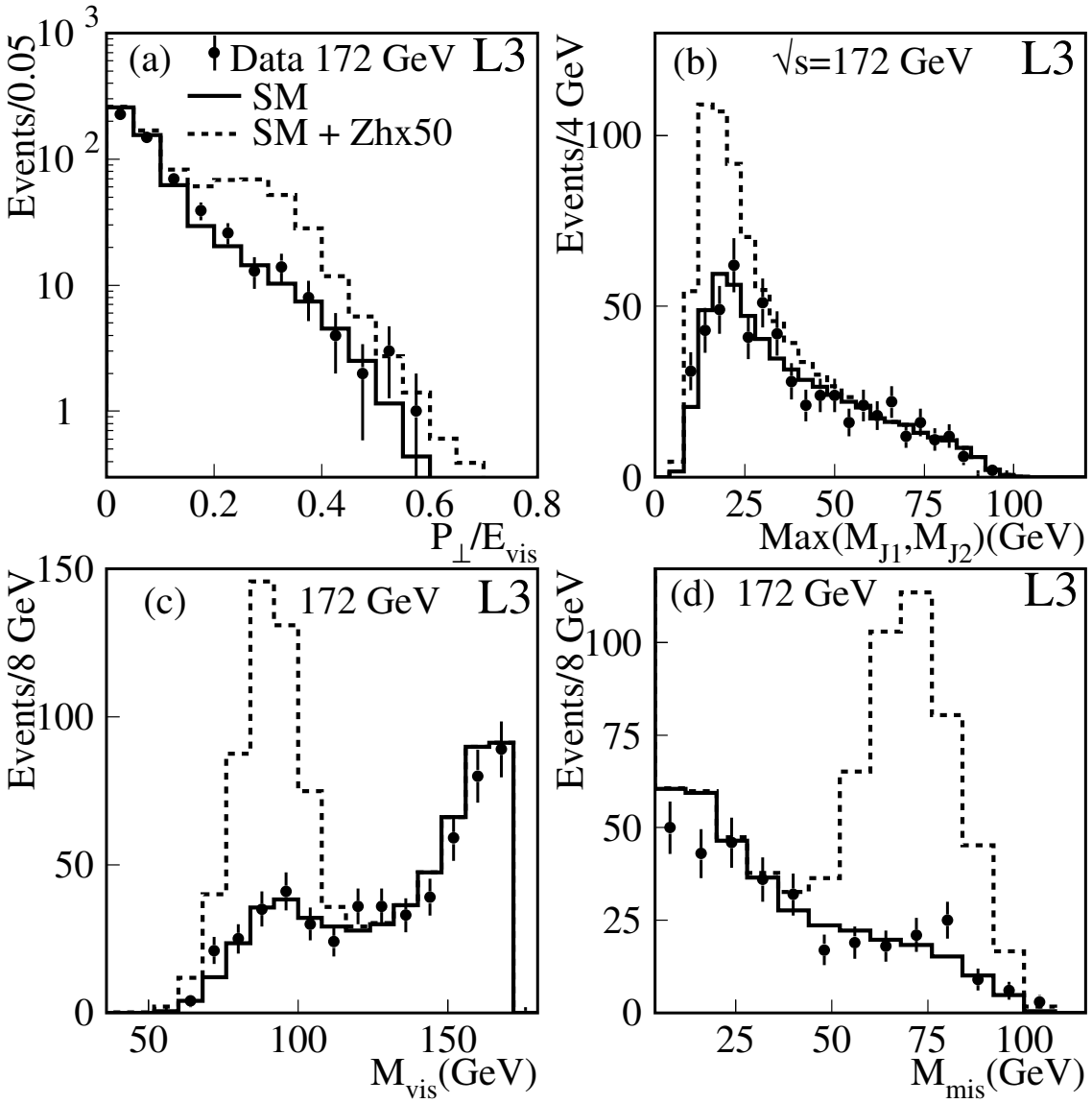

Figure 1: Distributions, at $\sqrt{s}$ = 172 GeV, after the hadronic preselection (see text) of (a) the transverse imbalance, (b) the maximum jet mass, when the event is reconstructed into two jets, (c) the visible mass and (d) the missing mass. In (d) only events with $M^2_{mis} \geq 16$ GeV^2 are shown. The data (dots) are compared to the sum of the Standard Model contributions (solid histogram) from fermion pair production plus four fermion production. The sum of the Standard Model (SM) and the Higgs signal (Zh) contributions for a 70 GeV Higgs is shown by the dashed histogram. The Higgs contribution is normalised to 50 times the actual luminosity, using the Standard Model Higgs production cross section.

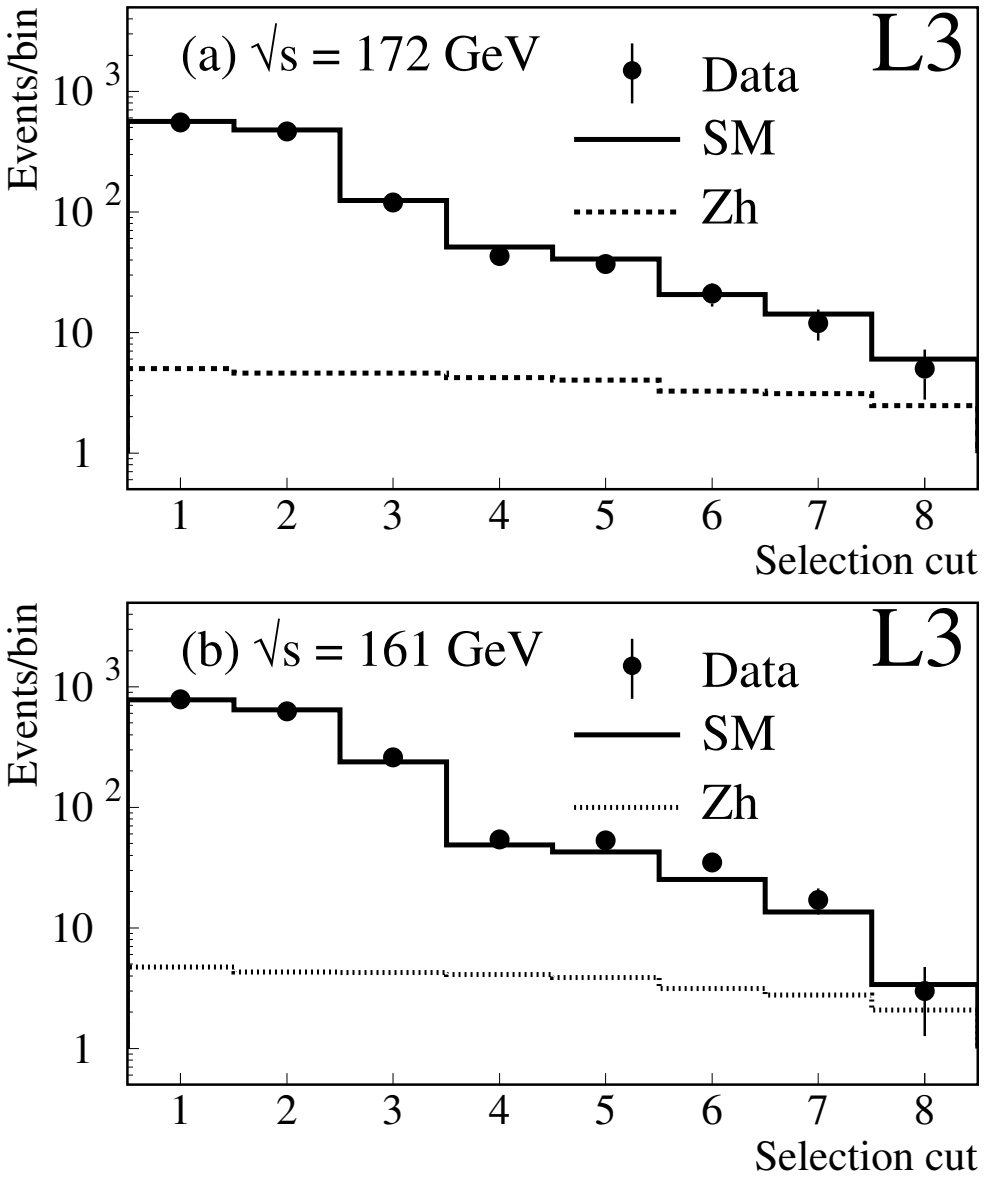

Figure 2: The number of events observed in the data (dots), after sequentially applying the selection cuts, at (a) $\sqrt{s} = 172$ GeV and (b) $\sqrt{s} = 161$ GeV, compared to the expectations for Standard Model production of fermion pairs plus four fermion final states (solid histogram). Superimposed is the number of events expected for a 70 (65) GeV Higgs signal, shown by the dashed (dotted) histogram, at $\sqrt{s} = 172$ (161) GeV. The Higgs distributions are normalised to the actual luminosities at the two centre-of-mass energies using the Standard Model Higgs production cross section.

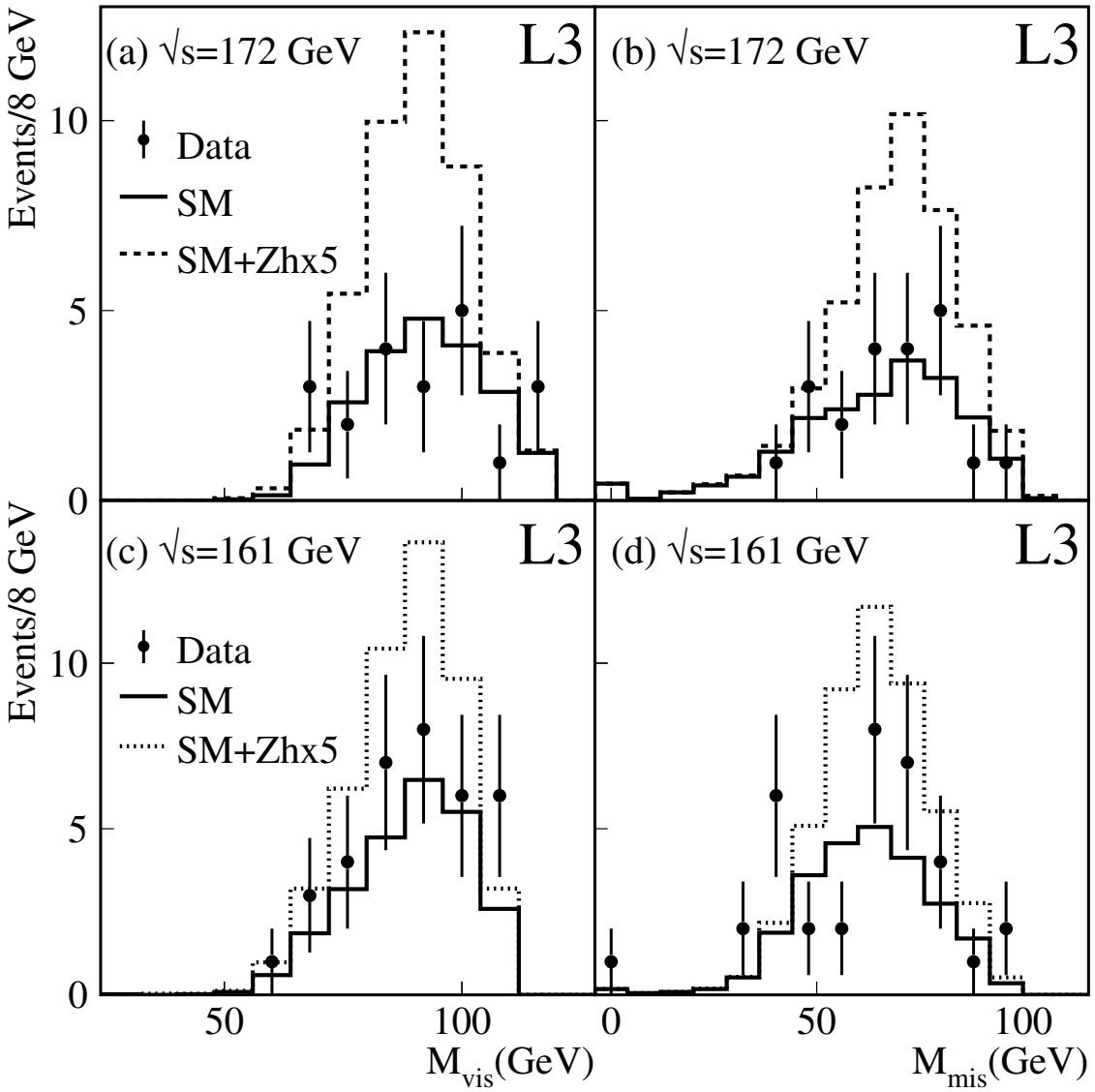

Figure 3: Distributions of the visible mass, (a), (c), and the missing mass, (b), (d), after selection cuts 1 through 6 (see text) at $\sqrt{s}$ = 172 GeV and 161 GeV for the data (dots) compared to the sum of the Standard Model contributions (solid histogram) from fermion-pair and four-fermion productions. The sum of the Standard Model (SM) and the Higgs signal (Zh) contributions for a 70 (65) GeV Higgs signal, at $\sqrt{s}$ = 172 (161) GeV, is shown by the dashed (dotted) histogram. The Higgs contribution is normalised to 5 times the actual luminosities using the Standard Model Higgs production cross section.

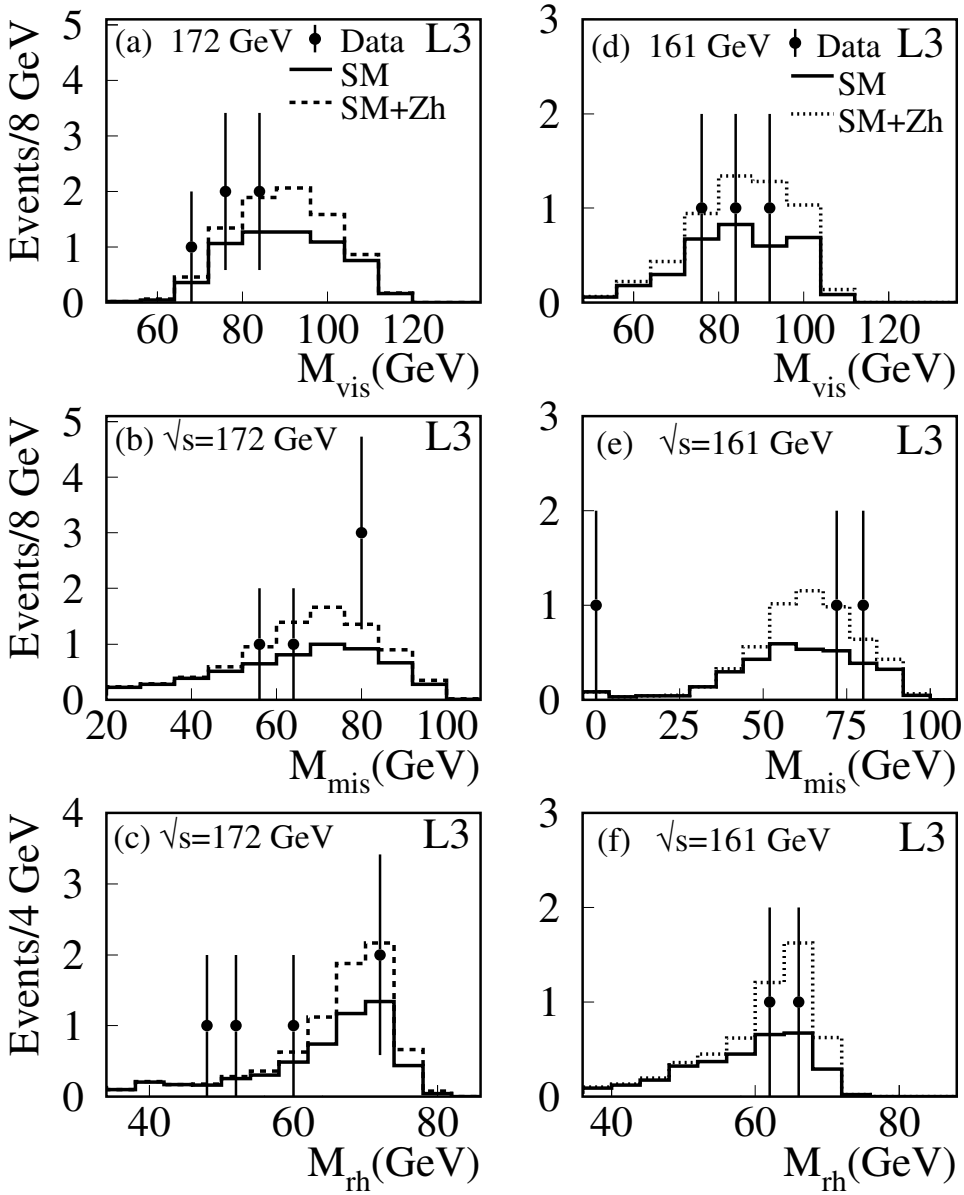

Figure 4: Distributions of the visible mass $M_{\rm vis}$, (a) and (d), the missing mass $M_{\rm mis}$, (b) and (e), and the reconstructed Higgs mass $M_{\rm rh}$, (c) and (f), at $\sqrt{s}$ = 172 GeV and 161 GeV. The data (dots) are compared to the sum of the Standard Model contributions (solid histogram). The sum of the Standard Model and the Higgs signal contributions, for a 70 (65) GeV Higgs at $\sqrt{s}$ = 172 (161) GeV, is shown by the dashed (dotted) histogram. The Higgs contribution is normalised to the actual luminosities using the Standard Model Higgs production cross section.

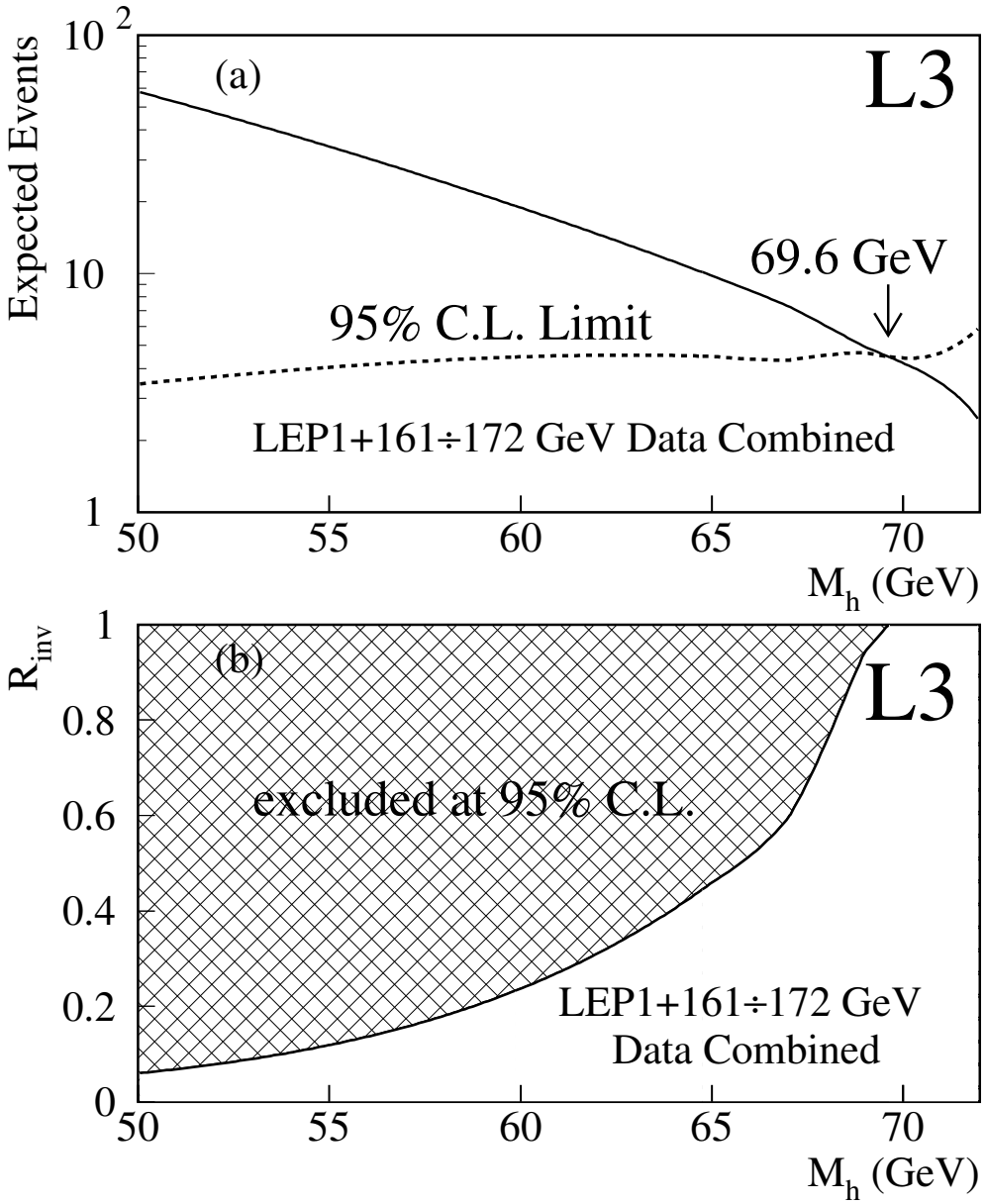

Figure 5: (a) The number of expected Higgs signal events (solid line), assuming Standard Model Higgs production cross section, and 100% decay branching fraction into invisible particles, and the 95% confidence level upper limit on the number of signal events (dashed line) as a function of the Higgs mass. This limit is set combining the $161 \div 172$ GeV with the LEP1 results of the search for invisible Higgs dacays. (b) Upper limit on $R_{\rm inv}$, the rate of invisible Higgs decays, relative to the Standard Model Higgs production rate.